Published in final edited form as:
Neuroimage. 2007 February 1; 34(3): 1084–1092.

Improved spatial localization of post-stimulus BOLD undershoot relative to positive BOLD

Fuqiang Zhao, **Tao Jin**, **Ping Wang**, and **Seong-Gi Kim**
Departments of Radiology and Neurobiology, University of Pittsburgh, Pittsburgh, PA, 15203, USA

Abstract

The negative blood oxygenation level dependent (BOLD) signal following the cessation of stimulation (post-stimulus BOLD undershoot) is observed in functional magnetic resonance imaging (fMRI) studies. However, its spatial characteristics are unknown. To investigate this, gradient-echo BOLD fMRI in response to visual stimulus was obtained in isoflurane-anesthetized cats at 9.4 T. Since the middle cortical layer (layer 4) is known to have the highest metabolic and cerebral blood volume (CBV) responses, images were obtained to view the cortical cross-section. Robust post-stimulus BOLD undershoot was observed in all studies, and lasted longer than 30 sec after the cessation of 40-60 sec stimulation. The magnitude of post-stimulus BOLD undershoot was linearly dependent on echo time with little intercept when extrapolating to TE = 0, indicating the T_2^* change is the major cause of the BOLD undershoot. The post-stimulus BOLD undershoot was observed within the cortex and near the surface of the cortex, while the prolonged CBV elevation was observed only at the middle of the cortex. Within the cortex, the largest post-stimulus undershoot was detected at the middle of the cortex, similar to the CBV increase during the stimulation period. Our findings demonstrate that, even though there is significant contribution from pial vessel signals, the post-stimulus undershoot BOLD signal is useful to improve the spatial localization of fMRI to active cortical sites.

Keywords

fMRI; post-stimulus undershoot; BOLD; Hemodynamic response; $CMRO_2$; Cortical layers; CBV; spatial localization

Introduction

Blood oxygenation level-dependent (BOLD)-based (Ogawa and Lee, 1990) functional magnetic resonance imaging (fMRI) has been a method of choice for visualizing neuronal activity in humans. Neuronal activation within the cerebral cortex leads to a series of physiologic alterations, including localized increase in cerebral blood flow (CBF), cerebral blood volume (CBV), and cerebral metabolic rate of oxygen ($CMRO_2$). These hemodynamic responses form the basis of this fMRI technique. Hence the spatial localization of fMRI maps is dependent on these physiological sources and the contribution of non-specific macrovessels. It is well-known that positive BOLD signal spreads out beyond neuronal active sites and is

Corresponding to: Fuqiang Zhao, Biomedical Imaging Technology Center, Coulter Dept of Biomedical Engineering at Georgia Tech and Emory University, 101 Woodruff Circle, Suite 2001, Atlanta, GA 30322, TEL: 404-712-2710, FAX: 404-712-2707, E-mail: fuqiangzhao@yahoo.com

sensitive to large draining vessels (Lai et al., 1993,Duong et al., 2000a,Duong et al., 2000b,Menon, 2002,Zhao et al., 2004,Zhao et al., 2006).

In addition to the positive BOLD signal, the post-stimulus BOLD undershoot is usually observed (Kwong et al., 1992,Frahm et al., 1996,Kruger et al., 1996,Buxton et al., 1998,Mandeville et al., 1999b,Yacoub et al., 2006). This can be attributed to one or a combination of three possible physiological sources: (i) an increased oxygen extraction rate due to the sustained post-stimulus elevation in $CMRO_2$ (Frahm et al., 1996,Kruger et al., 1996,Ances et al., 2001,Lu et al., 2004a,Yacoub et al., 2006), (ii) CBF undershoot after the cessation of stimulation (Hoge et al., 1999,Uludag et al., 2004), and (iii) the delayed recovery in venous CBV (Buxton et al., 1998,Mandeville et al., 1999a,Mandeville et al., 1999b). Even though the source of the post-stimulus BOLD undershoot has been extensively investigated, its spatial characteristics have not been examined possibly due to limited spatial resolution of previous fMRI studies. Spatiotemporal dynamics of post-stimulus BOLD signals can provide insight to the source of the post-stimulus BOLD signals and its potential utility for high-resolution brain mapping.

The primary aim of this work is to investigate the spatial localization of post-stimulus BOLD undershoot in the visual cortex of isoflurane-anesthetized cats at 9.4 T. To view the cortical cross-section with in-plane resolution of 312×312 μm^2, a 2-mm thick imaging slice was selected perpendicular to the cortical surface. Since the middle cortical layer is known to have the highest cytochrome oxidase activity, neural activity and density of synapses (Woolsey et al., 1996) at baseline, and the highest stimulation-induced changes in metabolism (Woolsey et al., 1996), CBF (Woolsey et al., 1996,Duong et al., 2000b) and CBV (Lu et al., 2004b,Harel et al., 2006,Zhao et al., 2006), the highest signal changes should occur at the middle of the cortex if the post-stimulus BOLD undershoot signals are specific to metabolic response and/or CBV response. To investigate whether post-stimulus BOLD undershoot signals indeed originate from a change in R_2^* ($=1/T_2^*$), four gradient-echo times (TEs) were used. To further investigate the spatial characteristics of the post-stimulus BOLD undershoot, the spatial localization of post-stimulus BOLD undershoot was compared with CBV response by re-processing the previously reported data with 156×156×1000 μm^3 resolution (Zhao et al., 2006).

Materials and Methods

Animal Preparation

Ten female adolescent cats (weight: 0.76-1.6 kg, 10-16 weeks old) were studied with approval from the Institutional Animal Care and Use Committee at the University of Pittsburgh Medical School. Cats were anesthetized with a ketamine (10-25 mg/kg) and xylazine (2.5 mg/kg) cocktail (i.m.). The cat was orally intubated and mechanically ventilated using a pressure-driven Kent ventilator (model: RSP-1002, CT) (~29-30 strokes/min) under isoflurane anesthesia (1-1.3% v/v) in a 2:1 N_2:O_2 mixture. An intravenous catheter was inserted into the cephalic veins to continuously infuse ~0.2 mg/kg/hr pancuronium bromide mixed in 5% dextrose Ringer's solution by infusion pump. The cat was placed in a cradle and restrained in normal postural position by a head holder, consisting of ear bars and bite bar. End-tidal CO_2 (Datex Omeda, Helsinki, Finland) was maintained in the range of 3.0 - 3.8%. During MRI experiments, end-tidal CO_2 were continuously recorded (MP150, BIOPAC Systems Inc., Goleta, CA). Rectal temperature was maintained at 38.5±0.5°C with a feedback hot water circulator.

Visual Stimulation

Binocular visual stimuli were presented from a video projector (NEC, model #: MT1055; resolution 1040×890) onto a rear-projection screen. The screen was positioned ~15 cm from the cat's eyes, covering about ~37° of the visual field. Visual stimuli consisted of square-wave high-contrast moving gratings (2 cycles/sec) with low spatial frequency (0.2 cycles/degree) at a selected orientation. During the pre- and post-stimulus periods, a stationary grating pattern with the same orientation was presented.

General MRI Experiments

All NMR experiments were performed on a 9.4 T/31-cm horizontal MRI system (Varian, Palo Alto, CA, USA). The actively shielded 12-cm-diameter gradient insert (Magnex, UK) operates at a maximum gradient strength of 40 gauss/cm and a rise time of 130 μs. A 1.6-cm diameter surface coil positioned on top of the cat head provided radiofrequency (RF) transmission and reception. The visual cortex was positioned in the iso-center of the magnet, and the magnetic field homogeneity was optimized by manual shimming. From multi-slice GE BOLD 'scout' fMRI and anatomical images, a 2-mm thick oblique coronal slice orthogonal to the surface of the visual cortex was chosen. This ensured that cortical depth-dependent structures would be similar at the posterior-anterior direction within this imaging slice. All subsequent experiments were conducted on this slice with a 2×2 cm^2 field of view (FOV) and a 2-mm thickness. T_1-weighted anatomical images were obtained to identify brain structures by the four-shot spin echo (SE) planar imaging (EPI) technique with an inversion time of 1.4 sec, TE of 17 ms, and repetition time (TR) for each segment of 5.4 s.

All four-TE fMRI images (n = 5 animals) were acquired with matrix size of 64×64 by single-shot GE EPI technique. The power level of the sinc-shaped RF pulse was adjusted to maximize signal intensity within the visual cortex. Echo times of 10, 15, 20 and 25 ms were interleaved in each run, which consisted of 30 × 4 (60 sec) control, **30 × 4** (60 sec) stimulation and 60 × 4 (120 sec) post-stimulus image acquisitions with TR of 0.5 s.

To compare post-stimulus responses of BOLD and CBV, we used high-resolution BOLD and CBV-weighted fMRI data presented previously (n = 5 animals) (Zhao et al., 2006). The method to acquire the data was described in detail elsewhere (Zhao et al., 2006). Briefly, high resolution (0.16×0.16 mm^2 in-plane resolution) of BOLD and CBV-weighted fMRI data were acquired in the same cat before and after 10 mg/kg MION injection with four segmented GE EPI. Each run consisted of 10 control, **10** stimulation, and 10 control image acquisitions with TR = 4 s. The rest time between each run is >2 minutes for raw data saving, reconstruction and cat recovering. The long time (>3 minutes) between the subsequent stimulation warranted the hemodynamic responses's return to baseline (Jin et al., 2006).

Data Analyses

Data were processed using Stimulate (Strupp, 1996) and MATLAB routines (Mathworks, Natick, MA). Color fMRI maps were overlaid on original baseline EPI images. Graphs were plotted with standard errors of means (SEM), and all others were reported as mean ± standard deviation (SD).

Image data from all repeated fMRI scans were averaged. Images with different TEs were acquired at different time points, and thus linear temporal interpolation was performed to take into account their different time origins. Statistical *t*-value maps were computed by comparing the experimental fMRI data acquired during the initial control period vs. data acquired during stimulation. The ROI including all activated pixels from BOLD fMRI with TE=20 ms was used for quantitative analysis of four-TE data. Percent changes of averaged signals were plotted

as a function of echo time. Since the percent signal change can be approximated as $\Delta S/S = -\Delta R_2^* \times TE + intercept$, the slope of the linearly fitted line is stimulation-induced $-\Delta R_2^*$ and the intercept is the non-T_2^* effect.

In order to examine spatiotemporal characteristics of BOLD and post-stimulus BOLD responses, four TE data were averaged (the rationale will be given later). Both TE-averaged data and high-resolution data were analyzed by two different approaches without any statistical threshold: generation of time-dependent subtraction maps (ΔS) and profile analysis of region of interest (ROI). ΔS maps were obtained by subtraction of average baseline image from stimulation-induced images on a pixel-by-pixel basis, and then displayed as a gray scale. To generate a signal profile in the cortical depth dimension, two quadrangular regions within the visual cortex were independently selected (one within each hemisphere) based on T_1-weighted anatomical images. Each ROI was ~3 pixels (~6 pixels for high-resolution data) wide along the dorsal flat surface of the cortex and ~6 pixels (~12 pixels for high-resolution data) in the cortical depth dimension (perpendicular to the dorsal surface). These ROIs were placed along the medial side of the white matter at the position where the cortical curvature was least and where the variations of the cortical profile along the depth dimension were minimal. The average distance within these quadrangular ROIs from the surface of the cortex to the gray/white matter boundary was determined in each animal. The signals at the same relative cortical depth, regardless of statistical criteria for activation, were averaged along the surface dimension. One profile was generated for each animal from the quadrangular ROIs in area 18. Cortical layer locations were assigned based on relative distances of those layers in area 18 (Payne and Peters, 2002).

Results

TE-dependence of the post-stimulus BOLD undershoot

To investigate the TE-dependence of BOLD fMRI, data was obtained with TE = 10, 15, 20 and 25 ms. Figs. 1A and 1B show anatomical T_1-weighted EPI image and conventional positive BOLD *t*-value map at TE = 20 ms of one animal. From the anatomical image (Fig. 1A), cortical surface (the green contours) and anatomical boundaries between gray and white matter (the black contours) were determined and then overlaid on Fig. 1B (background GE EPI image with activation map). No obvious spatial mis-registration was observed between Fig. 1A (which was acquired with four-shot SE EPI technique) and Fig. 1B (which was acquired with single-shot GE EPI technique) because they have a similar gradient train. However, in some regions, as indicated by cyan arrow in Fig. 1B, low signal intensity at the dorsal surface of the cortex in the single-shot GE image appears, which is likely due to susceptibility-induced dephasing around the large surface veins. The largest conventional positive BOLD signal changes (yellow pixels) were seen near the surface of the cortex (the green contours) and the lower cortical regions near the white matter (the black contours). This observation is consistent for all TE studies in five cats and with the previous high resolution GE BOLD studies at 9.4T (Harel et al., 2006,Zhao et al., 2006).

Time courses of four-TE BOLD fMRI signals were obtained from the same ROI (all activated pixels at TE = 20 ms, as shown in Fig. 1B). Average time courses from all five cats are shown in Fig. 1C. TE-dependent BOLD signal changes were observed. The conventional positive BOLD signal reached its peak at 9.1 ± 0.8 sec (n = 5) following the stimulus onset, and the post-stimulus BOLD undershoot reached the negative peak at 12.7 ± 1.5 sec (n = 5) following the cessation of the stimulus, which was significantly longer than the time-to-peak ($p < 0.002$). To recover the post-stimulus BOLD signal to a pre-stimulus baseline level, ≥ 40 sec is needed. This long recovery time is consistent with previous observations (Janz et al., 2001,Lu et al., 2004a).

To examine possible sources of the post-stimulus BOLD undershoot, Fig. 1D displays the plots of percentage signal changes vs. TE for all five cats. Both conventional positive BOLD (average signal of 8 ~ 60 sec after stimulus on) and post-stimulus undershoot (average signal of 12 ~ 36 sec after cessation of stimulation) signals demonstrate linear TE dependence (n = 5 animals, where R^2 values for individual data were all > 0.97). The average R_2^* change is -0.31 ± 0.06 sec^{-1} (n = 5) for the conventional positive BOLD signal and +0.26 ± 0.07 (n = 5) for the post-stimulus BOLD undershoot. The average intercept of conventional positive BOLD signal is 0.32 ± 0.13 % (n = 5), while the average intercept of BOLD post-stimulus undershoot is -0.07 ± 0.04 % (n = 5). For post-stimulus undershoot, the contribution from intercept is much smaller than the contribution from R_2^* change. Thus, the post-stimulus BOLD undershoot signal originates mostly from a change in R_2^*.

Since spatiotemporal characteristics were independent of TE (data not shown), all four-echo data were averaged for further studies. Statistical *t*-value maps of positive BOLD and post-stimulus BOLD undershoot were calculated by comparing the pre-stimulus control images with the images acquired during the stimulation (8 - 60 sec) and the images acquired during 12 - 36 sec after cessation of stimulation. Direct comparison of *t*-value maps by the same threshold is biased due to the different contrast-to-noise ratios (CNRs) of positive BOLD and BOLD undershoot signals, and thus 1000 pixels with the highest t-value were chosen by adjusting their thresholds individually. Figure 2 shows *t*-value maps of positive BOLD and post-stimulus BOLD undershoot from two cats. Consistent with previous observations (Fig. 1), pixels with high *t*-value in positive BOLD maps (yellow pixels Fig. 2) are in the area near the surface of the cortex (green contour) and in the lower cortical regions near the white matter (the black contours). Pixels with high *t*-value for post-stimulus undershoot are in the middle cortical region and the cortical surface (purple pixels in Fig. 2). The middle cortical area indicated by the red arrow has lower BOLD signal change, but higher post-stimulus undershoot.

Spatial localization of post-stimulus BOLD undershoot

To determine the spatiotemporal evolution of the BOLD signal, time-dependent ΔS maps were obtained. Figure 3 shows time-dependent BOLD ΔS maps obtained from TE-averaged data during stimulation and post-stimulation periods, and Figure 4 shows time-dependent BOLD and CBV-weighted ΔS maps obtained from high-resolution data. As previously shown, the highest positive BOLD signals were observed near the surface of the cortex (bright pixels near green contours) during the visual stimulation period (left column of Fig. 3 and Fig. 4A). Within the cortex, relatively uniform BOLD signal changes were initially observed (see Fig. 3A), but at later time points during 60-s stimulation, the BOLD signal in the middle of the cortex decreased almost to a pre-stimulus baseline level (see Fig. 3E). This can be due to dynamic uncoupling-to-coupling changes between CBF and $CMRO_2$ as observed by Frahm et al. (Frahm et al., 1996) and/or a slow venous CBV increase (Buxton et al., 1998,Mandeville et al., 1999a,Mandeville et al., 1999b). After the cessation of stimulation (right column of Fig. 3 and Fig. 4B-D), the post-stimulus undershoot appears in the middle of the cortex (dark pixels indicated by the red arrow) and near the surface of the cortex (see dark pixels near green contours). The significant undershoot is observed within 36 sec after cessation of stimulation (corresponding to Fig. 3F-H and 4B-D), which is consistent with the time courses of Fig. 1C. In all animals, similar results were observed.

In order to examine whether regions with large post-stimulus undershoots are at the middle of the cortex, CBV-weighted fMRI maps were compared (Figs. 4E-H). As shown previously, the maximum CBV-weighted fMRI signal changes (white pixels in Fig. 4E indicated by red arrow) followed the middle of the visual cortex, where the highest post-stimulus undershoot occurs (compare Figs. 4C-D and Fig. 4E). After cessation of stimulation, the sustained small CBV

increase was observed in middle cortex until 24-s post-stimulation (see Fig 4F and G). At ~28-36 sec after the offset of stimulation, CBV-weighted signal recovered to pre-stimulus baseline (Fig. 4H), while small post-stimulus BOLD signal was still detected (Fig. 4D and 3H).

To further examine the spatial localization of the conventional positive BOLD and post-stimulus BOLD undershoot fMRI maps, profiles of signal changes across cortical layers were obtained from ROIs without any statistical threshold. Averages of results from five animals' TE-average data were plotted as a function of depth from the surface of the cortex (Fig. 5A). Similarly, profiles of stimulation and post-stimulation results from high-resolution BOLD and CBV data (n = 5) are shown in Fig. 5B-C. Post-stimulus BOLD undershoot (Figs. 5A and 5C green triangles) has a peak at the middle of the cortex, where the highest CBV change occurs (Fig. 5B blue circles). Interestingly, the CBV-weighted signal was positive at the surface of the cortex during the post-stimulus period (blue circles in Fig. 5C), indicating the CBV decreases after cessation of stimulation at the surface of the cortex.

Discussion

Physiological source of post-stimulus BOLD undershoot

Our results of TE-dependence show that post-stimulus BOLD undershoot is linearly dependent on TE, with a very small negative intercept when TE is linearly extrapolated to 0, indicating that the apparent transverse relaxation rate change induced by blood susceptibility effect is a major source. Such blood susceptibility effect can be due to a sustained venous blood volume increase, and/or a decrease in venous oxygenation level. To determine which one is the dominant source of the post-stimulus BOLD undershoot, high-resolution BOLD and CBV-weighted fMRI was conducted in the same animal before and after MION injection. Even though the CBV-weighted fMRI signal reflects changes in total CBV (venous and arterial) rather than pure venous CBV change, the dominant source of post-stimulus BOLD undershoot can still be estimated by analysis of spatial characteristics of post-stimulus BOLD and CBV-weighted fMRI signals. Our results indicate that the detected post-stimulus undershoot of cat visual cortex is dominated by blood oxygenation decrease.

During the post-stimulus BOLD undershoot period, an increased CBV was observed at the middle of the cortex, while a decreased CBV change (see blue circles in Fig. 5C) was detected in the surface of the cortex. However, post-stimulus BOLD undershoots were observed at the middle and surface of the cortex. This indicates that the prolonged venous CBV recovery is not a major source of the post-stimulus BOLD undershoot at the surface of the cortex. Otherwise, a large arterial blood volume decrease is needed to compensate the venous blood volume increase, which has been suggested to not be the case (Yacoub et al., 2006). Furthermore, based on the measurement of CBF and CBV response in the visual cortex of cat (Jin et al., 2006), CBF and CBV responses in the cortical surface are similarly fast, indicating that the CBV response is dominated by arterial vessel dilation in the cortical surface. This MR observation is also supported by recent in vivo microscopic measurements of pial vessels during increased neural activity, which detect large stimulation-induced dilation in arterial blood vessels, but not in venous vessels (Tian et al., 2006). Since no venous vessel dilation is detected during stimulation in the cortical surface, there should be no post-stimulus elevated venous CBV there. Taken together, our observed post-stimulus BOLD undershoot in the surface of the cortex is not dominated by venous CBV increase.

In the middle cortical area, even if a delayed CBV recovery was observed after the cessation of stimulation, the CBV signal recovered more quickly to a pre-stimulus baseline level than the post-stimulus BOLD undershoot. Comparing Figs. 4C and D with Figs. 4G and H, it is obvious that there is a strong post-stimulus BOLD undershoot at >12 sec after the cessation of

the stimulation while the post-stimulus CBV response is very weak. When considering the BOLD signal contribution to CBV-weighted fMRI (Kennan et al., 1998), the actual post-stimulus CBV response is less than the observed CBV-weighted change. Thus, we can conclude that the prolonged venous CBV increase is not a major source of the post-stimulus BOLD undershoot in the middle cortical area under our experimental and physiological conditions in the cat visual cortex.

Alternatively, the post-stimulus BOLD undershoot can be due to a decrease in venous oxygenation level which can be caused by prolonged elevation of oxygen extraction which would be likely to occur in the middle cortex (Frahm et al., 1996,Ances et al., 2001,Lu et al., 2004a,Yacoub et al., 2006) and/or the post-stimulus CBF undershoot. Since deoxyhemoglobin from active sites drains into downstream vessels including intra-cortical and pial veins, the large post-stimulus BOLD undershoot was also observed at the surface of the cortex where the large pial veins reside,. This post-stimulus undershoot behaves in the same manner as the positive BOLD response - highly oxygenated venous blood originates mostly in the middle cortical area, and then is drained to the cortical surface where the highest signal change is observed.

Spatial specificity of post-stimulus BOLD undershoot

The improved localization of the post-stimulus BOLD undershoot to the middle cortical layers was observed. The post-stimulus BOLD undershoot is likely due to an increase in blood deoxygenation, which can be caused by combination of increased oxygen extraction and/or post-stimulus CBF undershoot, and a contribution from sustained venous CBV response. Thus, the spatial localization of post-stimulus BOLD undershoot is related to the specificity of $CMRO_2$, CBF and venous CBV signals. It is well-known that $CMRO_2$ response is specific to active sites (Lowel et al., 1987,Thompson et al., 2003,Lu et al., 2004a). Stimulation-induced CBF and CBV increases are also proved to have high spatial specificity (Duong et al., 2001,Lu et al., 2004b,Vanzetta et al., 2004,Zhao et al., 2005). Hence the contribution from post-stimulus elevated venous CBV should also be expected to have high spatial specificity. A post-stimulus elevated $CMRO_2$ causes a BOLD signal decrease, a post-stimulus elevated venous CBV causes a BOLD signal decrease, and a post-stimulus CBF decrease also causes a BOLD signal decrease. So all these three effects enhance each other to provide the high spatial specificity of post-stimulus BOLD undershoot within the cortex.

Careful observation of positive BOLD signal shows that the middle of the cortex has smaller signal changes than the upper and lower cortical layers. This has been commonly observed in our high-resolution BOLD studies (Zhao et al., 2006) and shown in high-resolution BOLD data reported by Harel et al. even though it was not mentioned (Harel et al., 2006). The spatial profile of BOLD signal across the cortex is dependent on spatial extents and profiles of the functional changes of CBF, $CMRO_2$, and venous CBV. Since an increase in $CMRO_2$ causes a decrease in BOLD signal, while an increase in CBF causes an increase in BOLD signal, the specificity of conventional positive BOLD signal is worse than that of $CMRO_2$, CBF or CBV signals (see also (Duong et al., 2000a)). Combination of high $CMRO_2$ and CBV responses at the middle of the cortex may explain a low BOLD response at the middle of the cortex.

In our studies, isoflurane was used as an anesthesia. Isoflurane's effect on isolated cerebral arterioles and intraparenchymal arterioles is known to cause vasodilation (Flynn et al., 1992,Farber et al., 1997), hence to increase baseline CBF (Masamoto et al., 2006). It is also found that Isoflurane reduces neural response (Martin et al., 2006,Masamoto et al., 2006) to stimulation. All these effects are likely to cause the BOLD fMRI response to be reduced compared to that under awake condition (Peetersa et al., 2001,Cohen et al., 2002). However, the general pattern of BOLD fMRI response under anesthesia is similar to that of awake

condition (Martin et al., 2006) so our interpretation of animal studies is likely to be applicable to awake human studies. Since the post-stimulus BOLD undershoot originates mostly from a decrease in venous oxygenation level induced by an elevated oxygen consumption, its localization should be more specific than positive BOLD signals. Improved spatial localization to the parenchyma is likely to be achieved in human studies by using the post-stimulus BOLD undershoot. However, when the gradient-echo technique is used, extravascular signals around the large draining vessel are also contributed to the BOLD undershoot, reducing the spatial specificity. Thus, to remove extravascular BOLD signals around the large vessels, the spin-echo approach can be implemented at high magnetic fields (Lee et al., 1999,Zhao et al., 2006).

In conclusion, regardless of the signal source, the post-stimulus BOLD undershoot improves the spatial specificity to the middle cortical layers compared to the conventional positive BOLD signal. Although its magnitude and duration are closely dependent on the type and duration of stimuli, the post-stimulus BOLD undershoot is often observed in human fMRI studies and may be used for the improvement of spatial specificity.

Acknowledgements

Supported by NIH (EB03375, EB03324, EB02013, NS44589). We thank Christopher Glielmi for careful proofreading of this manuscript.

Reference

Ances BM, Buerk DG, Greenberg JH, Detre JA. Temporal dynamics of the partial pressure of brain tissue oxygen during functional forepaw stimulation in rats. Neurosci Lett 2001;306:106–110. [PubMed: 11403969]

Buxton RB, Wong EC, Frank LR. Dynamics of blood flow and oxygenation changes during brain activation: The baloon model. Magn Reson Med 1998;39:855–864. [PubMed: 9621908]

Cohen ER, Ugurbil K, Kim S-G. Effect of basal conditions on the magnitude and dynamics of the blood oxygenation-level dependent fMRI response. J Cereb Blood Flow and Metab 2002;22:1042–1053. [PubMed: 12218410]

Duong TQ, Kim D-S, Ugurbil K, Kim S-G. Spatiotemporal Dynamics of the BOLD fMRI Signals: Toward Mapping Submillimeter Cortical Columns Using the Early Negative Response. Magn Reson Med 2000a;44:231–242. [PubMed: 10918322]

Duong TQ, Kim D-S, Ugurbil K, Kim S-G. Localized cerebral blood flow response at submillimeter columnar resolution. Proc Natl Acad Sci USA 2001;98:10904–10909. [PubMed: 11526212]

Duong TQ, Silva AC, Lee S-P, Kim S-G. Functional MRI of Calcium-Dependent Synaptic Activity: Cross Correlation with CBF and BOLD Measurements. Magn Reson Med 2000b;43:383–392. [PubMed: 10725881]

Farber NE, Harkin CP, Niedfeldt J, Hudetz AG, Kampine JP, Schmeling WT. Region-specific and Agent-specific Dilation of Intracerebral Microvessels by Volatile Anesthetics in Rat Brain Slices. Anesthesialogy 1997;87:1191–1198.

Flynn NM, Buljubasic N, Bosnjak ZJ, Kampine JP. Isoflurane produces endothelium-independent relaxation in canine middle cerebral arteries. Anesthesiology 1992;76:461–467. [PubMed: 1539859]

Frahm J, Kruger KD, Merboldt KD, Kleinschmidt A. Dynamic uncoupling and recoupling of perfusion and oxidative metabolism during focal brain activation in man. Magn Reson Med 1996;35:143–148. [PubMed: 8622575]

Harel N, Lin J, Moeller S, Ugurbil K, Yacoub E. Combined imaging-histological study of cortical laminar specificity of fMRI signals. Neuroimag 2006;29:879–887.

Hoge RD, Atkinson J, Gill B, Crelier GR, Marrett S, Pike GB. Stimulus-Dependent BOLD and Perfusion Dynamics in Human V1. Neuroimage 1999;9:573–585. [PubMed: 10334901]

Janz C, Heinrich SP, Kornmayer J, Bach M, Hennig J. Coupling of Neural Activity and BOLD fMRI Response: New Insights by Combination of fMRI and VEP Experiments in Transition From Single Events to Continuous Stimulation. Mag Reson Med 2001;46:482–486.

Jin, T.; Wang, J.; Zhao, F.; Wang, P.; Tasker, M.; Kim, S-G. Spatiotemporal characteristics of BOLD, CBV and CBF responses in the cat visual cortex; Proc 14th Annual Meeting; ISMRM, Seatle. 2006; p. 2762

Kennan RP, Scanley BE, Innis RB, Gore JC. Physiological basis for BOLD MR signal changes due to neuronal stimulation: Separation of blood volume and magnetic susceptibility effects. Magn Reson Med 1998;40:840–846. [PubMed: 9840828]

Kruger G, Kleinschmidt A, Frahm J. Dynamic MRI sensitized to cerebal blood oxygenation and flow during sustained activation of human visual cortex. Magn Reson Med 1996;35:797–800. [PubMed: 8744004]

Kwong KK, Belliveau JW, Chesler DA, Goldberg IE, Weisskoff RM, Poncelet BP, Kennedy DN, Hoppel BE, Cohen MS, Turner R, Cheng H-M, Brady TJ, Rosen BR. Dynamic Magnetic Resonance Imaging of Human Brain Activity during Primary Sensory Stimulation. Proc Natl Acad Sci USA 1992;89:5675–5679. [PubMed: 1608978]

Lai S, Hopkins AL, Haacke EM, Li D, Wasserman BA, Buckley P, Friedman H, Meltzer H, Hedera, Friedland R. Identification of vascular structures as a major source of signal contrast in high resolution 2D and 3D functional activation imaging of the motor cortex at 1.5T: preliminary results. Magn Reson Med 1993;30:387–392. [PubMed: 8412613]

Lee S-P, Silva AC, Ugurbil K, Kim S-G. Diffusion-weighted spin-echo fMRI at 9.4 T: microvascular/tissue contribution to BOLD signal change. Magn Reson Med 1999;42:919–928. [PubMed: 10542351]

Lowel S, Freeman B, Singer W. Topographic organization of the orientation column system in large flat-mounts of the cat visual cortex: a 2-deoxyglucose study. J Comp Neurol 1987;255:401–415. [PubMed: 3819021]

Lu H, Golay X, Pekar J, van Zijl PC. Sustained Poststimulus Elevation in Cerebral Oxygen Utilization after Vascular Recovery. J Cereb Blood Flow Metab 2004a;24:764–770. [PubMed: 15241184]

Lu H, Patel S, Luo F, Li S-J, Hillard CJ, Ward B, Hyde JS. Spatial Correlations of Laminar BOLD and CBV Responses to Rat Whisker Stimulation with Neuronal Activity Localized by Fos Expression. Magn Reson Med 2004b;52:1060–1068. [PubMed: 15508149]

Mandeville JB, Marota JJA, Ayata C, Moskowitz MA, Weisskoff RM, Rosen BR. MRI measurement of the temporal evolution of relative CMRO2 during rat forpaw stimulation. Magn Reson Med 1999a; 42:944–951. [PubMed: 10542354]

Mandeville JB, Marota JJA, Ayata C, Zaharchuk G, Moskowitz MA, Rosen B, Weisskoff R. Evidence of a Cerebrovascular Postarteriole Windkessel With Delayed Compliance. J Cereb Blood Flow and Metab 1999b;19:679–689. [PubMed: 10366199]

Martin C, Martindale J, Berwick J, Mayhew J. Investigating neural-hemodynamic coupling and the hemodynamic response function in the awake rat. Neuroimag 2006;32:33–48.

Masamoto K, Kim T, Fukuda M, Wang P, Kim S-G. Relationship between neural, vascular, and BOLD signals in isoflurane-anesthetized rat somatosensory cortex. Cereb Cortex. 2006In Press.

Menon RS. Postacquisition suppression of large-vessel BOLD signals in high-resolution fMRI. Magn Reson Med 2002;47:1–9. [PubMed: 11754436]

Ogawa S, Lee TM. Magnetic Resonance Imaging of Blood Vessels at High Fields: in Vivo and in Vitro Measurements and Image Simulation. Magn Reson Med 1990;16:9–18. [PubMed: 2255240]

Payne, BR.; Peters, A. The Concept of Cat Primary Visual Cortex. In: Payne, BR.; Peters, A., editors. The Cat Primary Visual Cortex. Academic Press; 2002. p. 1.-129.

Peetersa RR, Tindemansa I, De Schutterb E, Van der Lindena A. Comparing BOLD fMRI signal changes in the awake and anesthetized rat during electrical forepaw stimulation. Mag Reson Imag 2001;19:821–826.

Strupp JP. Stimulate: a GUI based fMRI analysis software package. Neuroimage 1996;3:S607.

Thompson JK, Peterson MR, Freeman RD. Single-Neuron Activity and Tissue Oxygenation in the Cerebral Cortex. Science 2003;299:1070–1072. [PubMed: 12586942]

Tian, P.; Devor, A.; Nishimura, N.; Teng, IC.; Dale, AM.; Kleinfeld, D. NeuroScience. Atlanta, USA: 2006. 2006. Spatiotemporal profile of single-vessel hemodynamic response to a somatosensory stimulus in relation to maps of underlying neuronal activity; p. 363.-366.

Uludag K, Dubowitz DJ, Yoder EJ, Restom K, Liu TT, Buxton RB. Coupling of cerebral blood flow and oxygen consumption during physiological activation and deactivation measured with fMRI. Neuroimage 2004;23:148–155. [PubMed: 15325361]

Vanzetta I, Slovin H, Omer DB, Grinvald A. Columnar Resolution of Blood Volume and Oximetry Functional Maps in the Behaving Monkey. Neuron 2004;42:843–854. [PubMed: 15182722]

Woolsey TA, Rovainen CM, Cox SB, Henegar MH, Liang GE, Liu D, Moskalenko YE, Sui J, Wei L. Neuronal units linked to microvascular modules in cerebral cortex: response elements for imaging the brain. Cereb Cortex 1996;6:647–660. [PubMed: 8921201]

Yacoub E, Uguribl K, Harel N. The spatial dependence of the poststimulus undershoot as revealed by high-resolution BOLD- and CBV-weighted fMRI. J Cerb Blood Flow Metabolism 2006;26:634–644.

Zhao F, Wang P, Hendrich K, Kim S-G. Spatial Specificity of Cerebral Blood Volume-weighted fMRI Responses at Columnar Resolution. Neuroimage 2005;27:416–424. [PubMed: 15923128]

Zhao F, Wang P, Hendrich K, Uguribl K, Kim S-G. Cortical layer-dependent BOLD and CBV responses measured by spin-echo and gradient-echo fMRI: Insights into hemodynamic regulation. Neuroimag 2006;30:1149–1160.

Zhao F, Wang P, Kim S-G. Cortical Depth-Dependent Gradient-Echo and Spin-Echo BOLD fMRI at 9.4T. Magn Reson Med 2004;51:518–524. [PubMed: 15004793]

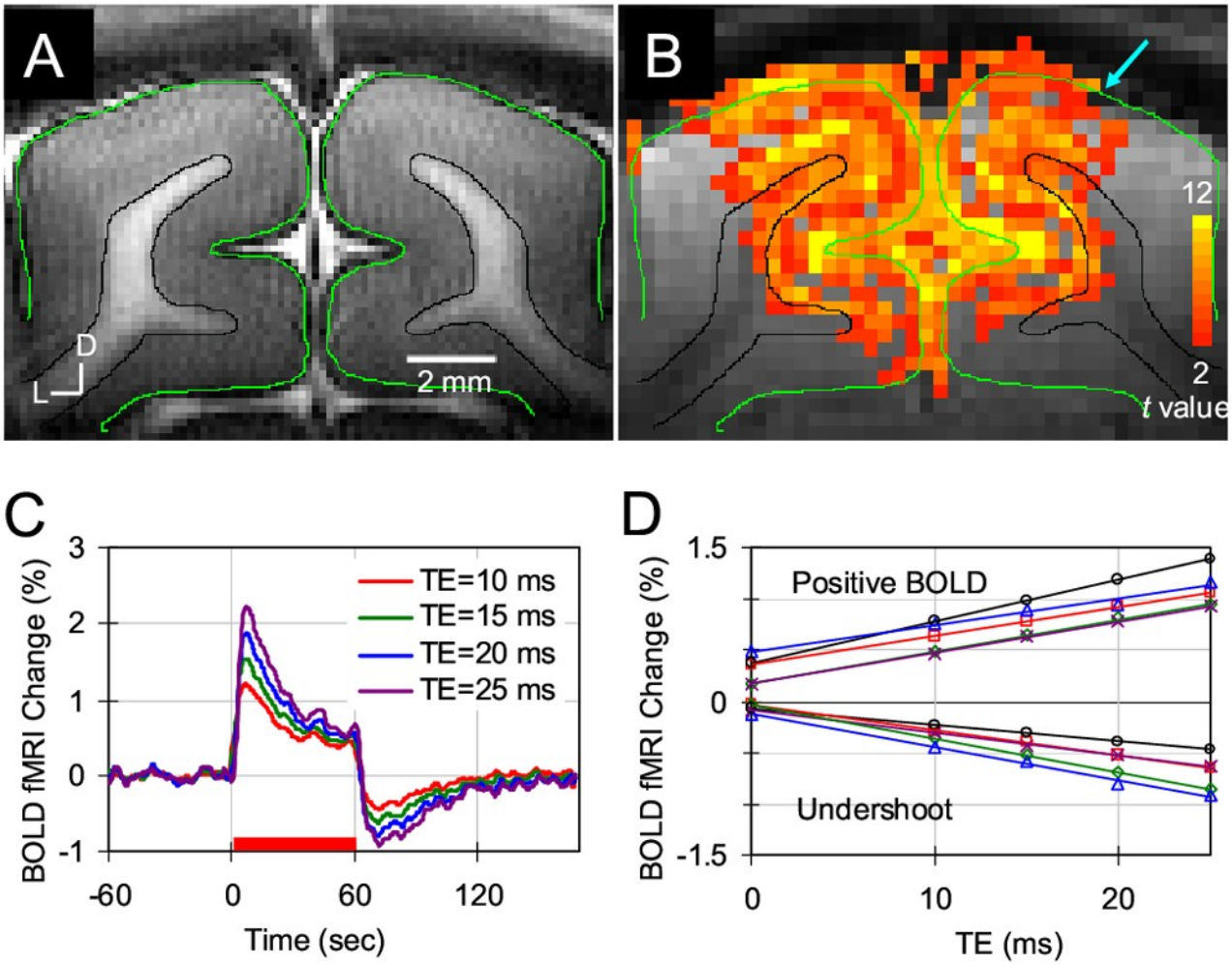

Figure 1.

TE-dependence of BOLD fMRI signals. T_1-weighted anatomical image (**A**) and conventional positive functional *t*-value map (**B**) of one animal are shown. The cortical surface is outlined in green contours and white matter boundaries are delineated by black contours from anatomic image. These were overlaid on images in Figs. 1B, 2 and 3. A cyan arrow in (**B**) indicates signal intensity loss due to susceptibility-induced dephasing around the large surface veins. The statistical *t*-value threshold was set to 2.0 with a minimum cluster size of 4 pixels ($p < 0.01$). D: dorsal, L: lateral. **(C)** Average time courses of five animals were plotted for four different TEs. A red bar under the time courses indicates the 60 sec visual stimulation period. (**D**) The percentage signal change vs. TE for positive BOLD and post-stimulus BOLD undershoot is shown in individual animals (n = 5). Additionally, linearly fitted lines are also drawn.

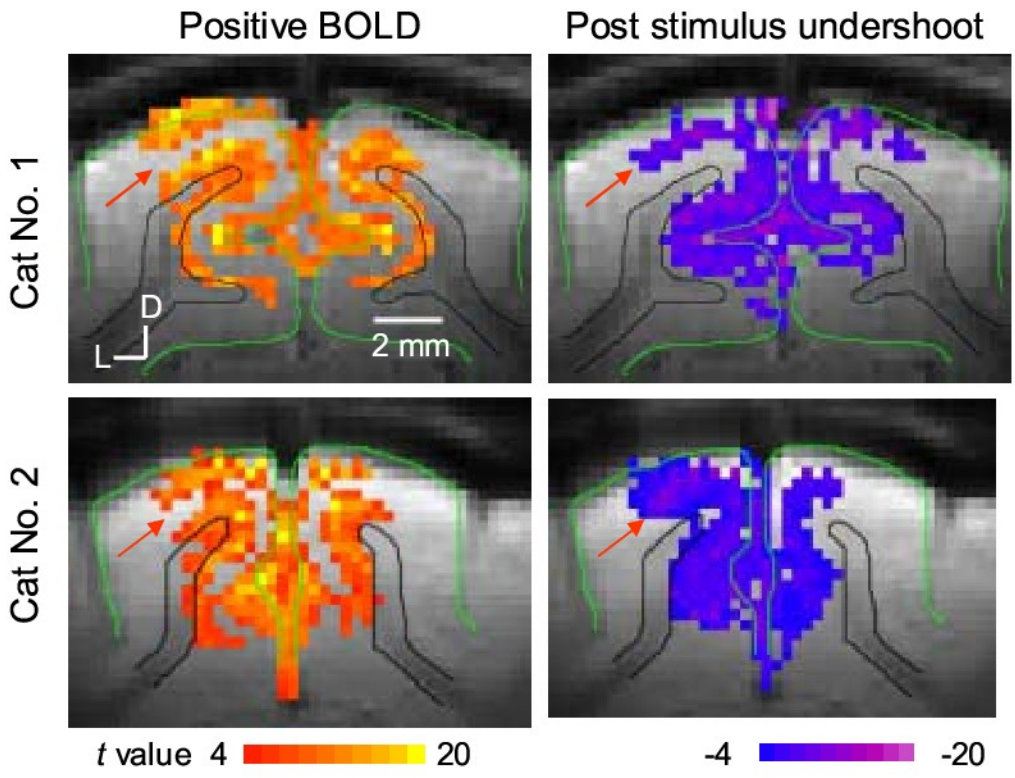

Figure 2.

BOLD maps vs. post-stimulus BOLD undershoot maps. *t*-value maps of positive BOLD (left) and post-stimulus BOLD undershoot (right) were obtained from TE-averaged data in two cats. Images acquired during a stimulation period except initial 8 sec and during 12-36 sec after cessation of stimulation were used for positive and post-stimulus BOLD maps, respectively. To minimize the influence of different CNRs for positive BOLD and post-stimulus BOLD undershoot, 1000 pixels with highest *t* values were chosen by adjusting the threshold individually. D: dorsal, L: lateral.

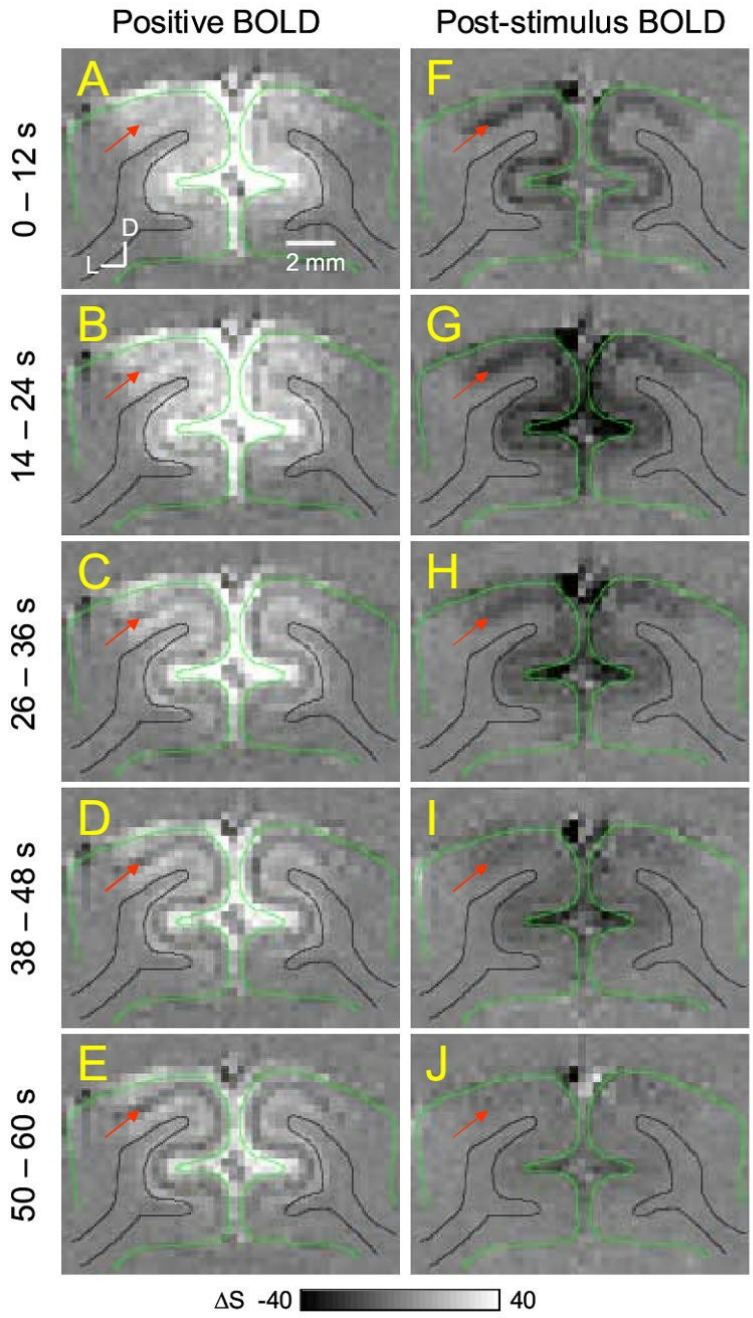

Figure 3.

Time-dependent subtraction maps of conventional positive BOLD and post-stimulus BOLD signals. Functional subtraction maps are absolute changes from the pre-stimulus baseline level. Maps were calculated during the different time periods (indicated by the numbers left of the maps) after onset (left column) and cessation (right column) of stimulation. Red arrows indicate the middle of the cortex. Clearly, highest post-stimulus BOLD undershoot is observed in middle of the cortex, as well as the cortical surface (dark pixels in **F-I**). Green contour: cortical surface; black contour: white matter boundary; D: dorsal, L: lateral. The unit of gray scale bars is the multiple of the standard deviation within the noise area outside the brain.

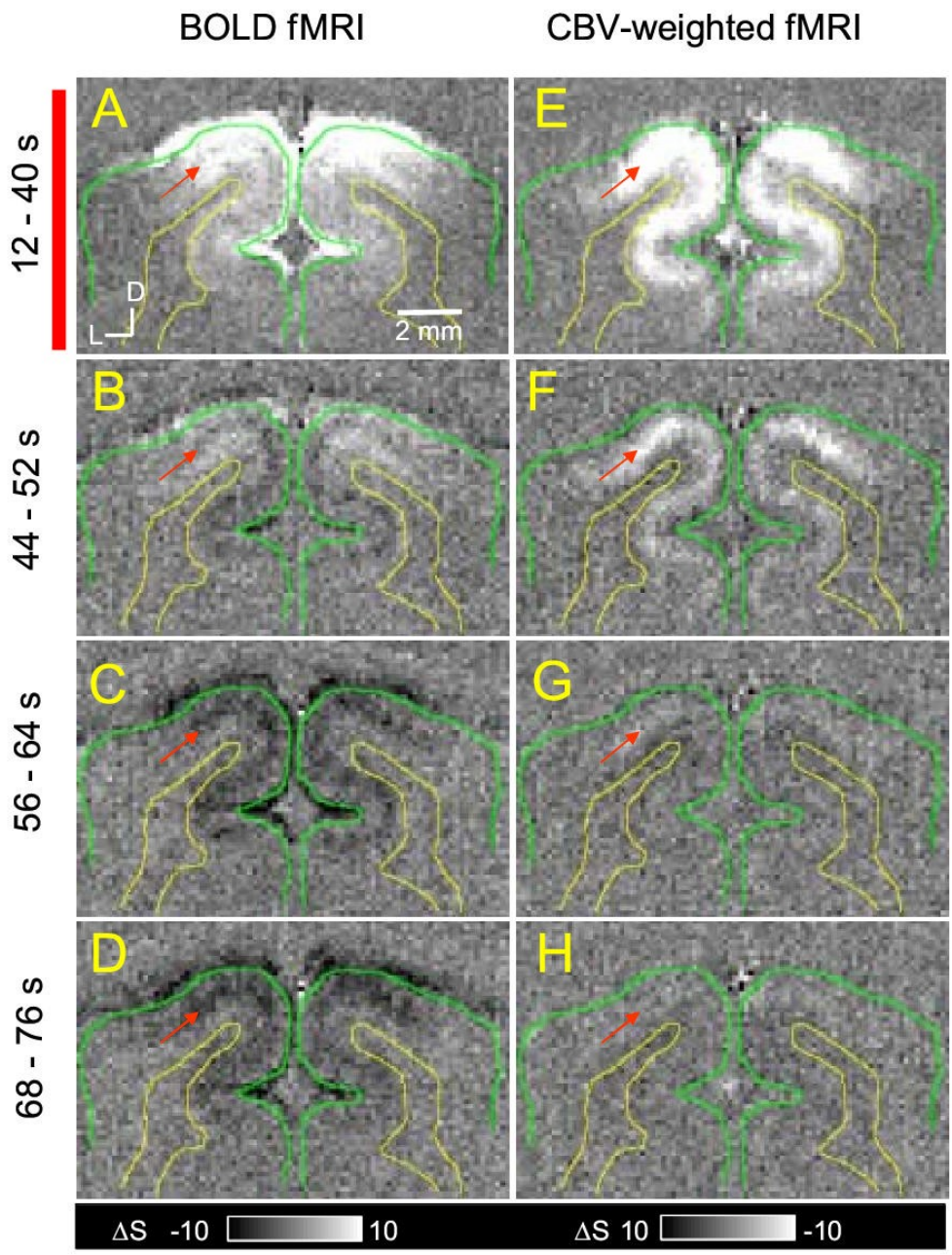

Figure 4.

Time-dependent subtraction maps of BOLD vs. CBV-weighted fMRI. BOLD (left column) and CBV-weighted (right column) subtraction maps are shown as absolute signal changes from pre-stimulus baseline levels. Maps were calculated during the steady-state stimulation condition (12 s - 40 sec after the onset of 40-s long stimulation, the red bar indicates stimulation) (**A** and **E**), an initial post-stimulus period (44-52 sec) (**B** and **F**), and two later post-stimulus periods (56-64 s and 68-76 s after the termination of stimulation) (**C** and **G**, **D** and **H**, respectively). Bright pixels in BOLD indicate positive signal changes, while those in CBV-weighted fMRI indicate a decrease in MRI signal and consequently an increase in CBV. The unit of gray scale bars is the multiple of the standard deviation within the noise area outside

the brain. Red arrows indicate the middle of the cortex. Clearly, post-stimulus BOLD undershoot was observed (**C** and **D**). Green contour: cortical surface; yellow contour: white matter boundary; D: dorsal, L: lateral.

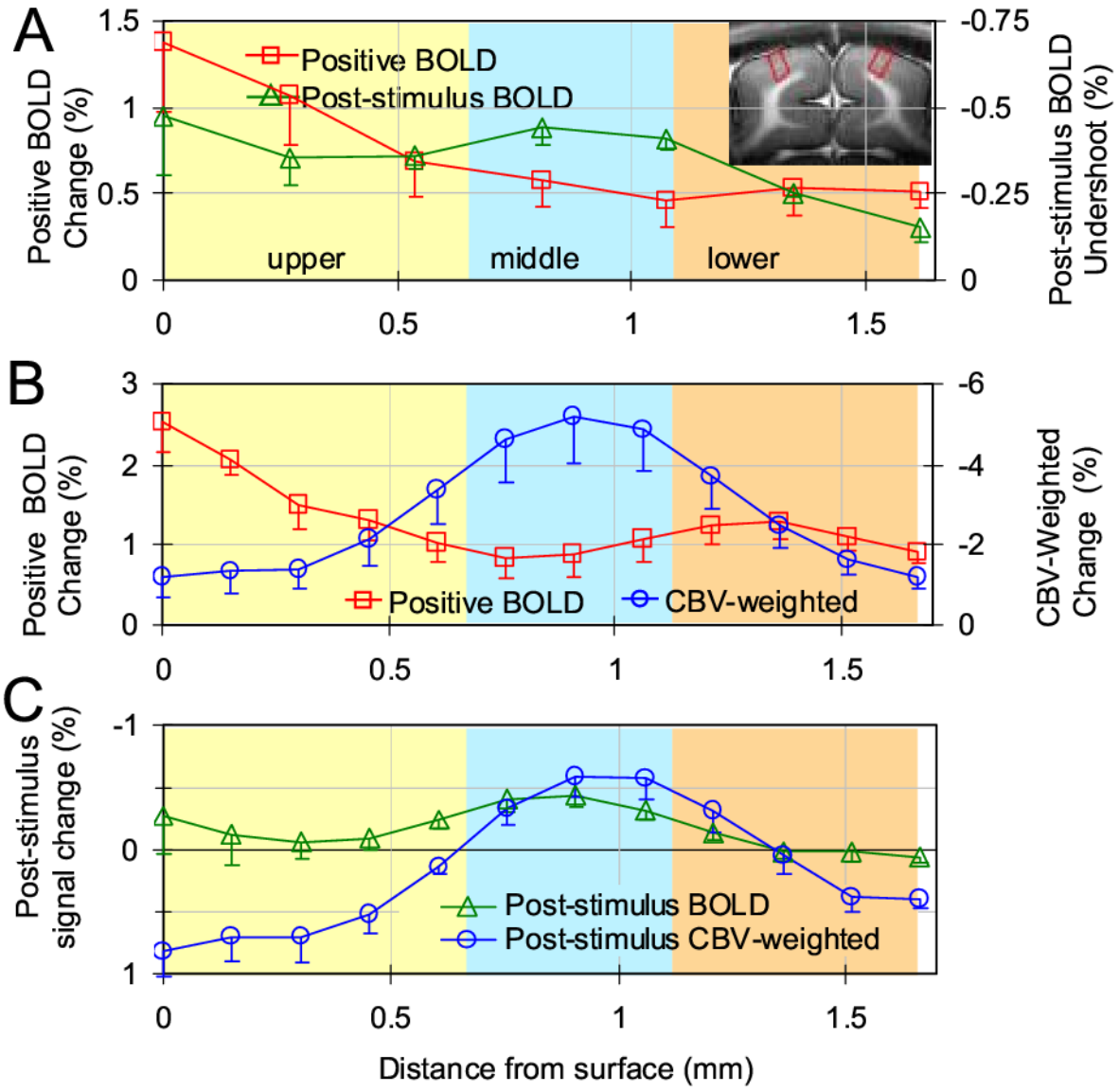

Figure 5.

Average profiles of BOLD and CBV-weighted fMRI signals across the cortex. Cortical depth dependent profile was generated for each animal from the quadrangular ROIs in area 18 (e.g., two red quadrangular ROIs in inset image), then data was averaged across all animals. Post-stimulus data was obtained from 12-36 s after the cessation of stimulation, while stimulation data was obtained from entire stimulation period except initial 8 seconds. TE-average data are shown in **A**, while high-resolution BOLD and CBV data during stimulation and post-stimulation periods are shown in **B** and **C**, respectively. The surface of the cortex is at zero, with cortical depth represented by increasing distances. Approximate location of cortical layers was determined by relative distances of those layers in area 18 (Payne and Peters, 2002) and is differentiated by colored bands. Negative change in CBV-weighted fMRI indicates an increase in CBV. The middle of the cortex has the highest stimulation-induced

CBV increase as well as highest post-stimulus BOLD undershoot. For clarity, only one side of the error bars (SEM) is shown.